Design and Evaluation of Haptic Interface Wiggling Method for Remote Commanding of Variable Stiffness Profiles

Schol, Jasper ; Hofland, Jelle; Heemskerk, Cock J.M.; Abbink, David A.; Peternel, Luka

DOI
10.1109/ICAR53236.2021.9659476

Publication date
2021

Document Version
Accepted author manuscript

Published in
Proceedings of the 2021 20th International Conference on Advanced Robotics (ICAR)

Design and Evaluation of Haptic Interface Wiggling Method for Remote Commanding of Variable Stiffness Profiles

Jasper Schol[1,2], Jelle Hofland[1], Cock J.M. Heemskerk[1], David A. Abbink[2], and Luka Peternel[2,*]

***Abstract*— Unlike many traditional stiff position-controlled robots, new collaborative robots interact with humans and operate in an environment that is often unpredictable and unknown. For safe and effective executions of manipulation tasks within such an environment, the robot requires to modulate its compliance. Therefore, the human operator must have a system that enables an intuitive demonstration of compliance skills to the robot. Ideally, this should also be possible through teleoperation in order to have the ability to demonstrate skills at a distance, such as in remote home care applications or any other scenario where the skilled operators are not physically present all the time. Existing state-of-the-art methods for remote demonstration of impedance skills only enable limited modulation of the stiffness matrix, or they are too complex and cumbersome for practical applications. This research tries to overcome these limitations and proposes a teleoperated stiffness commanding method that enables a complete modulation of the stiffness matrix in 3 degrees of freedom. The method uses the same haptic device hardware as used for controlling the robot manipulator motion, hence it does not require extra specialised equipment for stiffness commands. By wiggling the endpoint of the haptic device, the stiffness is commanded to the robot and also fed back to the operator through haptic and visual feedback. To evaluate the performance and acceptance of the system, we performed a user study where the participants had to demonstrate various interaction behaviour to the remote robot. The results show how varying system parameters (i.e., degrees of freedom, orientation, and size of the stiffness commands) influence the performance of the system and user acceptance.**

I. Introduction

Traditionally, industrial robots are stiff and position controlled, without the ability to adjust dynamic properties of the interaction. In combination with a well organised and known environment, this simple method is effective in autonomous and repetitive manipulation tasks, such as assembly in a production line. However, robots that work in unstructured and unpredictable environments or are interacting with humans require dynamic control in order to efficiently deal with complex interaction challenges. In this respect, impedance control gives robots the ability to adapt the properties of dynamic interaction with the environment [1].

Besides pre-programming, there are two main types of approaches to demonstrate or command the impedance skills to the robot: kinaesthetic guidance and teleoperation. In the first approach, the impedance parameters can be inferred through the data obtained by kinaesthetic guidance. For example, the method in [2] infers variable impedance skills from the measured force during kinaesthetic teaching. In [3], [4], the impedance is inferred through the variability in demonstrated kinematic trajectories; small variability in motion implies precision and thus high impedance, and vice-versa. While these methods do not require special interfaces, the operator can not control the impedance directly and might lead to undesirable parameters. For example, the motion through a narrow section, while in contact with the environment, has a small variability due to the environment constraint, and if the object is fragile, then high stiffness can lead to unsafe interaction forces [5]. Furthermore, kinaesthetic guidance requires physical presence of the human operator, which limits its use in applications such as remote home care. Therefore, teleoperation approach might often be preferred over pure autonomy or kinaesthetic guidance. There are also methods that can learn compliant motion directly from teleoperated demonstrations [6], [7], however, these too do not give the operator a direct control over the impedance.

In [8], the concept of tele-impedance was introduced, where surface electromyography (sEMG) measured the muscle activation of the operator to estimate human arm stiffness through offline calibration. The human endpoint stiffness was then superimposed to the robot impedance controller to command its impedance parameters in real-time. This sEMG approach was later on also used to teach the impedance skills to robots [9], [10]. However, these methods all require complex offline identification techniques to find the sEMG to stiffness mapping, which is operator-specific and typically only locally valid (in the identified arm pose). Simplifications were introduced in [9], [11], however sEMG is still a rather complicated system with wearable sensors and time-consuming calibration procedures. Additionally, when force-feedback is involved with sEMG interface [12], [13], there is a coupling between the force-feedback and the commanded impedance that takes away some direct control [14].

A fundamentally different approach to tele-impedance is to use the operator's grip force as an interface to command stiffness. The interface in [15] measured the force of grip on the handle of the master device by pressure sensors. The measured force was then linearly mapped to the commanded robot stiffness and damping. A different approach was introduced in [5], where the impedance was commanded by the position of the button on a handheld control interface. The methods [15] and [5] are more practical compared to sEMG, however they enable only control of a limited degrees of freedom (DoF), while the stiffness matrix has many DoF that are related to magnitude and orientation. Therefore, some aspects of the stiffness matrix must be coupled to a single

[1]Heemskerk Innovative Technology B.V., Delft, The Netherlands
[2]Delft Haptics Lab, Cognitive Robotics, Delft University of Technology, Delft, The Netherlands
*Corresponding author (e-mail: l.peternel@tudelft.nl)

control DoF and independent modulation is not possible.

The methods in [16], [17] proposed to use kinaesthetically induced perturbation to command impedance to the robot. This technique relies on physically wiggling the robot structure around its reference trajectory to modulate the stiffness in the three translational DoF. However, this method requires close physical interaction to move the robot and therefore remote demonstration or control is not possible. Furthermore, if the robot is large, physical interaction and movements are not easy. Finally, environment constraints can prevent the manipulator to be moved in a certain direction which can only be solved by commanding the robot with an offset in trajectory [17]. Nevertheless, this method does provide the possibility to vary all aspects of the stiffness matrix without using sEMG.

Given the limitations of the existing methods, this work designs and evaluates a novel stiffness commanding interface that allows the operator to provide remote demonstration of varying stiffness profiles in 3 DoF, where the three translational DoF can be varied in the direction (stiffness matrix eigenvectors) and magnitude (stiffness matrix eigenvalues). To make the interface suited for a real-world practical application, it is also important that the interface is easy to implement and does not use wearable devices or calibration precedes (i.e., limitations of sEMG). In addition, demonstration or control of stiffness should not be dependent on the environment constraints or kinematic trajectory. Additionally, the interface must be accepted by the operator such that stiffness behaviour can be easily and intuitively programmed.

Similar to [16], [17], the proposed method is based on perturbations around the kinematic reference trajectory in order to provide stiffness commands. Different from [16], [17], the proposed method does not induce perturbations by physically wiggling the robot. Instead, the haptic master device of teleoperation setup is used to make virtual perturbations. During the reference motion trajectory, the operator is moving a virtual marker around the current end-effector position of the robot by wiggling the haptic device. The larger the distance between the virtual marker and the end-effector (amplitude), the lower the stiffness, and the more compliant the end-effector of the robot will become in that direction. The commanded stiffness is updated online and fed back to the operator through a visualisation of compliance ellipsoid[1], and by providing stiffness related forces from the haptic device. Therefore, the operator sees and feels the stiffness changes, which helps him/her to estimate to what extent the commanded stiffness is successful with respect to what was intended. After the stiffness profile is demonstrated in a safe simulation environment, the robot can use the obtained stiffness profile in order to autonomously execute the task in real-life.

The main contribution of this paper is a new teleoperation based stiffness commanding method that allows direct modulation of all aspects of the stiffness matrix for 3 translational DoF. The proposed method was evaluated by a user study in terms of performance and acceptance in various conditions.

[1]Compliance ellipsoid in an inverse of stiffness ellipsoid.

II. Method Design

The main objective of the proposed system is to enable human operators to remotely demonstrate new interaction skills to the robot. Fig. 1 shows the system overview with the most important software blocks, signals, and apparatus. The key element is the new stiffness commanding interface for varying the stiffness parameter of the remote robot's impedance controller. This work assumes an already established or learned kinematic trajectory $\boldsymbol{x}_c$ and no assumptions are made on how it was obtained (e.g., it can be done remotely through the same haptic device that is used for stiffness demonstration). Additionally, during the stiffness demonstration in simulation, the impedance controller is temporarily bypassed to facilitate the creation of the stiffness profile through remote demonstration.

A. Stiffness commands from perturbations

The proposed demonstration method is intended to command stiffness for the 3 translation DoF through wiggling of a haptic device. Therefore, the requirements for the hardware setup is a haptic device with at least 3 DoF. The stiffness matrix $\boldsymbol{K} \in \mathbb{R}^{3\times3}$ gives a relationship between the contact forces and position errors, and we define it to be inversely proportional to a covariance matrix from the demonstration. This covariance matrix is constructed based on a perturbation signal that is created by the operator while moving the haptic device in the robot base frame, which is aligned with the world frame. By wiggling a virtual marker point $\boldsymbol{x}_m \in \mathbb{R}^{3\times1}$ around the current robot end-effector position $\boldsymbol{x} \in \mathbb{R}^{3\times1}$, a perturbation vector $\tilde{\boldsymbol{x}}$ can be found for each time step i as

$$\tilde{\boldsymbol{x}}_i = \boldsymbol{x}_i - \boldsymbol{x}_{m,i}. \tag{1}$$

The perturbation vector is stored over time in a data matrix $\boldsymbol{\Xi}^{\tilde{\boldsymbol{x}}\times L}$. From this data matrix, a covariance matrix $\boldsymbol{\Sigma}_i \in \mathbb{R}^{3\times3}$ is constructed. Here $L = T \cdot dt = \frac{T}{f_s}$ is the total amount of stored data points in the data matrix and hence the length of the sliding temporal window, where T is the time span of the window in seconds and f_s the frequency in Hz at which the software runs. As time progresses with time step dt, a new perturbation vector will be appended while the earliest vector will be removed from the data matrix. Therefore at time $t = t_1$, the data matrix contains the perturbation vectors in the range $[(t_1 - T),\ t_1]$ for $t_1 > T$. From this data matrix, the symmetric and positive definite (SPD) covariance matrix is found according to

$$\begin{aligned} \boldsymbol{\Sigma}_i &= \frac{1}{L}\sum_{i}^{L}(\tilde{\boldsymbol{x}}_i - \boldsymbol{\mu})(\tilde{\boldsymbol{x}}_i - \boldsymbol{\mu})^T, \\ \boldsymbol{\mu}_i &= \frac{1}{L}\sum_{i}^{L}\tilde{\boldsymbol{x}}_i, \end{aligned} \tag{2}$$

where $\boldsymbol{\mu} \in \mathbb{R}^{3\times1}$ is the average of the perturbation vectors in the data matrix. The three variances corresponding to the x, y and z-axis are presented on the diagonal of the covariance matrix, and the off-diagonal elements represent

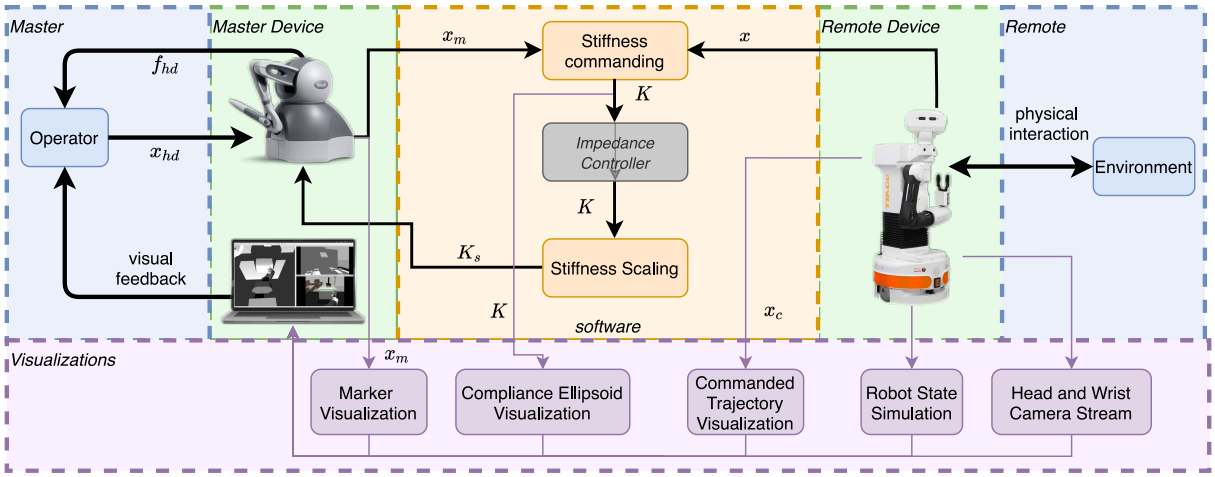

Fig. 1. System overview containing the most important software blocks, signals, and apparatus. The operator and the remote environment (blue sections) interact with the master and remote devices, respectively (green sections). The yellow section contains the software blocks and signals and the purple section shows the visualisation based on the important signals or robot sensors. Since no impedance (compliant) controller is implemented, the stiffness command K is directly connected to the stiffness scaling.

the covariance (coupling terms) between them. The next step is to set the covariance matrix inversely proportional to the stiffness matrix. Therefore, the direction and the magnitude should be found. Since the covariance matrix is a SPD matrix, eigendecomposition gives

$$\boldsymbol{\Sigma}_i = \boldsymbol{Q}\boldsymbol{\Lambda}\boldsymbol{Q}^T, \tag{3}$$

where $\boldsymbol{Q} \in \mathbb{R}^{3\times3}$ is a matrix containing the orthonormal eigenvectors (direction) and $\boldsymbol{\Lambda} \in \mathbb{R}^{3\times3}$ is a diagonal matrix composed of the eigenvalues $\lambda_i,\ i = 1,2,3$ (magnitude along the eigenvectors). We take eigenvectors from (3) and use them to construct the stiffness matrix as

$$\boldsymbol{K}_i = \boldsymbol{Q}\boldsymbol{\Gamma}\boldsymbol{Q}^T, \tag{4}$$

where $\boldsymbol{\Gamma}$ is a diagonal matrix of which the diagonal elements γ_i are defined to be the inverse to the square root of the diagonal elements of matrix $\boldsymbol{\Lambda}$, such that $\sigma_i = \sqrt{\lambda_i}$. The inverse relation for each diagonal element $\gamma(\sigma_i)$ is given by

$$\gamma(\sigma_i) = \begin{cases} \underline{K} & \sigma_i > \bar{\sigma} \\ \bar{K} - \frac{\bar{K}-\underline{K}}{\bar{\sigma}-\underline{\sigma}}(\sigma_i - \underline{\sigma}) & \underline{\sigma} \leq \sigma_i \leq \bar{\sigma}, \\ \bar{K} & \sigma_i < \underline{\sigma} \end{cases} \tag{5}$$

where σ_i is a measure of the amplitude of the perturbations (wiggles), and the minimum and maximum allowed perturbations $\underline{\sigma}$ and $\bar{\sigma}$ are tunable parameters. Since the diagonals γ_i of $\boldsymbol{\Gamma}$ should be bounded between the stiffness limits of the impedance controller, the stiffness diagonal γ is set inversely proportional to the perturbations measure σ. Therefore, the minimum and maximum allowed perturbation $[\underline{\sigma},\ \bar{\sigma}]$ is related to the minimum and maximum allowed stiffness limits of the impedance controller. The minimum and maximum stiffness is denoted by $[\underline{K},\ \bar{K}]$.

B. Visual feedback

Since stiffness commands are given using a remote-demonstration setup, it is important to have a good understanding of the remote robot and the environment. Additionally, to understand the system itself, visual cues are known to improve user acceptance and performance in Haptic Shared Control systems [18], [19]. To design the visual feedback system, we divided the operator's screen in 3 sections (see Fig. 2). The right-top side of the screen shows a camera stream from the robot's head camera, and the right-bottom shows the end-effector camera stream. The left side of the screen provides a simulated environment based on robot sensors. Here, the current robot state and additional visualisations of the signals are presented. The figure also shows the task of opening a microwave door.

The simulated environment includes 1) a model of the current robot state and 2) a point cloud that shows the environment constructed from the depth camera. In the simulated view, 3) the commanded end-effector trajectory is visualised to help in understanding the future motion of the end-effector. Furthermore, 4) the virtual marker is presented by the red sphere that is controlled by the endpoint of the haptic device. By moving the marker away from the end-effector, the marker color gradually changes from green to red providing a sense of depth. Finally, 5) the compliance ellipsoid is used to visualise the demonstrated stiffness and to help operators understand the effect of the input motion commands on the stiffness. Although the compliance ellipsoid is the inverse of a stiffness ellipsoid, the choice is made to visualise compliance, since this naturally matches the movement of the virtual marker $\boldsymbol{x}_m$. For example, if the operator wiggles the haptic device along the z-axis, the compliance ellipsoid forms a cigar shaped ellipsoid with the long axis aligned with the z-axis. This is intuitive since the long axis forms in the line of movement from the wiggling motion, resulting in lower stiffness along the z-axis.

C. Haptic feedback

Typically haptic feedback generated by the master device is used to feel the forces from the remote robot. In this work however, we use a different method to provide haptic feedback; the demonstrated manipulator stiffness is

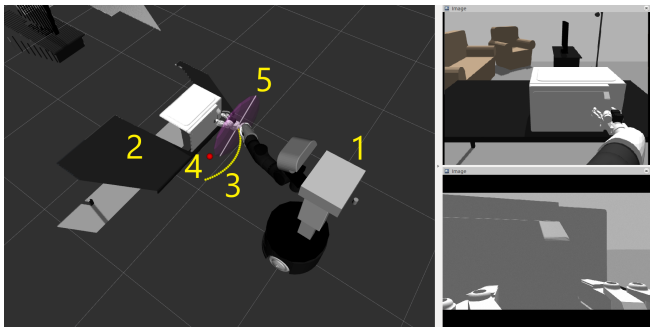

Fig. 2. The left picture shows an overview of the simulated remote environment. The top-right and bottom-right pictures show the visual feedback provided to the operator based on the head and wrist camera streams. The task mimics the process of opening the door of a microwave.

explicitly made observable through the haptic device by scaling the commanded stiffness and using this to produce a virtual stiffness force. If the endpoint of the haptic device moves away from its zero position, the virtual stiffness force pulls it back to the zero position, similar to how an impedance controlled manipulator would move back to its equilibrium trajectory. Therefore, the operator can sense the effects of the demonstrated stiffness directly without an actual impedance controller being present. This allows commanding of stiffness even for simulated motion where contact forces are absent. Since the operator evaluates the stiffness directly, it allows for quick adjustments during the motion. Additionally when a fixed stiffness is set (e.g. from earlier demonstrations), it also allows users to feel and improve upon the earlier commanded stiffness. It is important to convey this information haptically since this is how people naturally evaluate stiffness [16]. Furthermore, it supplements the compliance ellipsoid visualisation since it can be seen and felt simultaneously.

The virtual stiffness force is calculated by multiplying the scaled-down manipulator stiffness $\boldsymbol{K}_s \in R^{3\times3}$ with the deviation of haptic device from its zero position. To set (or limit) the force range that the haptic device can produce, the stiffness should be scaled to ensure that the haptic device uses the full or a defined range of force. This is done by defining the maximum allowed deviation $\bar{x}_{hd}$ of the haptic device and the minimum and maximum force limits (for maximum haptic device deviation). $[\underline{f}_{hd},\ \bar{f}_{hd}]$ of the haptic device. Subsequently, the minimum and maximum allowed stiffness for the haptic device deviation is defined as

$$\begin{aligned} \underline{K}_{hd} &= \frac{\underline{f}_{hd}}{\bar{x}_{hd}}, \\ \bar{K}_{hd} &= \frac{\bar{f}_{hd}}{\bar{x}_{hd}}. \end{aligned} \tag{6}$$

By relating the minimum and maximum manipulator stiffness limits $[\underline{K},\ \bar{K}]$ to the minimum and maximum allowed haptic device stiffness limits, the scaled down stiffness can be found.

In order to scale the stiffness matrix $\boldsymbol{K}$, eigenvalue decomposition of the stiffness matrix has to be performed such that the eigenvalues can be scaled. Using the eigenvalues of

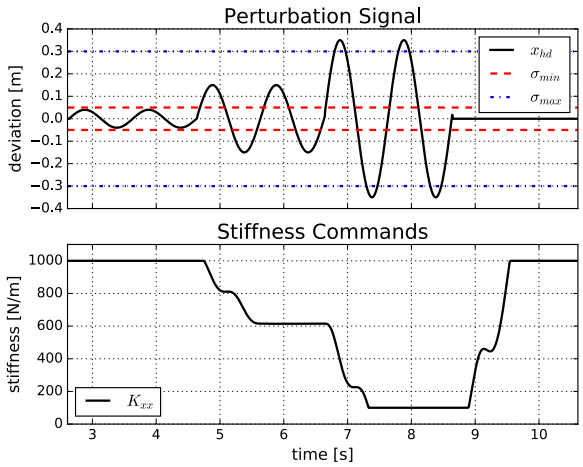

Fig. 3. The top plot shows a sinusoidal perturbation signal along the x-direction and the bottom plot shows the resulting stiffness commands.

(4), the diagonal matrix $\boldsymbol{K}_{s,e}$ with the scaled eigenvalues is given by

$$\boldsymbol{K}_{s,e} = \underline{\boldsymbol{K}}_{hd} + \frac{\bar{K}_{hd} - \underline{K}_{hd}}{\bar{K} - \underline{K}}(\boldsymbol{\Gamma} - \underline{\boldsymbol{K}}), \tag{7}$$

where $\underline{\boldsymbol{K}}_{hd}$, $\underline{\boldsymbol{K}}$ and $\bar{\boldsymbol{K}}$ are diagonal matrices with on the diagonals $\underline{K}_{hd}$, $\underline{K}$, $\bar{K}$ respectively. Once again, using (4) the scaled stiffness matrix is found using the eigenvectors of the decomposition as

$$\boldsymbol{K}_s = \boldsymbol{Q}\boldsymbol{K}_{s,e}\boldsymbol{Q}^T, \tag{8}$$

Subsequently, the force feedback is calculated by

$$\boldsymbol{f}_{hd} = \boldsymbol{K}_s\boldsymbol{x}_{hd}, \tag{9}$$

where $\boldsymbol{f}_{hd} \in \mathbb{R}^{3\times1}$ is the virtual stiffness force produced by the haptic device and $\boldsymbol{x}_{hd} \in \mathbb{R}^{3\times1}$ is its endpoint deviation away from the zero position.

D. Stiffness behaviour

This section shows how the perturbation signal (operator input) influences the stiffness commands and how the parameters influence the system. Given the stability stiffness limits of the manipulator, parameters that influence the stiffness commands are the amount of data points in the sliding window $L = dt \times T = \frac{T}{f_s}$, and the parameters $\bar{\sigma}$, $\underline{\sigma}$. The sliding window length along with the frequency rate of the software determines the time it takes to completely refresh the window with data points. The time it takes to refresh the window mainly influences the rate of stiffness changes during the demonstration. Therefore, a large window and a high frequency rate correspond to slow rate of change of stiffness, and vice-versa. The parameters $\underline{\sigma}$, $\bar{\sigma}$ represent the standard deviation of the data in the data matrix $\boldsymbol{\Xi}^{\tilde{\boldsymbol{x}}\times L}$ and are related to minimum and maximum allowed deviation of the haptic device endpoint. Given the inverse relation of (5), motion below $\underline{\sigma} = 0.0707$ increases the stiffness to the maximum limit $\bar{K} = 1000$ N/m and above $\bar{\sigma} = 0.3$ to a minimum limit

$\underline{K} = 100$N/m of the manipulator. This effect is shown in Fig. 3.

The sliding window length and software frequency are $L = 100$ and $f_s = 100$ Hz. Therefore, the time it takes to completely refresh the window is $T = 1$ s. This can be observed by looking at the top and bottom graphs of Fig. 3. In the top graph at approximately 4.5 seconds a sinusoidal with an amplitude larger than the threshold starts. After 1 second the window is completely refreshed with new data points, and this is shown in the bottom graph, where the stiffness has flattened to 600 N/m at 5.5 seconds.

III. Experiment

An important aspect of the method is that non-expert operators can use it to demonstrate stiffness skills. We evaluated the method by an experimental user study, where the operator was instructed to recreate various compliance ellipsoids (representing the stiffness matrix) as accurately as possible. The quantitative aspects were evaluated based on the trial time and by comparing the ellipsoid demonstrated by the operator to the reference ellipsoid. The reference ellipsoids were varied in size, orientation, and required either 1 or 2 DoF commands. Note that the references were provided as 3D ellipsoids, therefore the user had to reproduce 3D ellipsoids through either 1 DoF or 2 DoF command mode. In the 1 DoF command mode, different stiffness axes were demonstrated sequentially one by one, while in the 2 DoF mode multiple axes were demonstrated simultaneously. The subjective aspects of user acceptance were evaluated by the *van der Laan* questionnaire [20].

First, we hypothesised that 1 DoF stiffness commands have higher performance scores, compared to 2 DoF stiffness commands. To describe task complexity we used the theoretical model in [21], which implies that simultaneous actions contribute to increased overall task complexity. Thus, the level of task complexity in executing simultaneous actions (as in 2 DoF mode) may exceed the capacity of the individual operator, which leads to a lower performance.

Second, we hypothesised that commanding compliance in the horizontal (or transverse) plane yields lower performance scores, as compared to commands in the vertical (or frontal) plane. The reason being that commands in the horizontal plane require the operator to predominantly use the visual feedback that has a top-down view of the horizontal plane, while natural human eye view is in vertical plane. Therefore, misalignment exists between the operator view and the control input, which does not exist in the vertical plane. In [22] it was shown that to improve teleoperation, a setup should minimise control and view rotations. Additionally, the manipulability of the human arm changes with the arm configuration [23], and can be different when operating in the horizontal plane and in the vertical plane. While no research is found that directly relates the effect of human arm manipulability on different planes on teleoperated task performance, it could contribute to performance increase or decrease.

Finally, we hypothesised that larger shapes take more time to demonstrate, compared to small shapes. To create large shapes, the haptic device endpoint has to travel a greater distance, resulting in more time needed per trial. No effect was expected in terms of similarity between the reference and user demonstrated stiffness ellipsoid.

A. Participants

Eight male participants (age: $M = 25.15$, $SD = 2.53$) volunteered and were included in the experiment. All participants gave their prior consent and the experiment was approved by the Human Research Ethics Committee of the Delft University of Technology.

B. Experiment setup and protocol

The experiments were performed on a remote-demonstration setup consisting of a 3D Systems Touch Haptic Device, which measured operator's position commands and provided force feedback about the remote robot. The remote robot was simulated in Gazebo. The computer screen in front of the participant provided the visual feedback. Before starting the experiment each participant was provided a description of the setup, method and task instructions. A familiarisation trial was performed prior to the experiment. In the experiment, the participant had to demonstrate a given stiffness profile in four different conditions, where each condition was preceded with a practice run to get used to that specific condition. After the final condition, the participants were asked to fill in a *van der Laan* questionnaire along with four additional questions complementing the questionnaire:

- What did you like or find helpful?
- What did you find undesirable or hard?
- Which condition did you find most difficult and why?
- Do you have any remarks?

The experiment conditions were defined as a combination of 1 or 2 DoF stiffness commands, and whether they were commanded in a horizontal or vertical plane, leading to the following notations: *1 DoF – horizontal*, *1 DoF – vertical*, *2 DoF – horizontal* and *2 DoF – vertical*. Within each condition, the ellipsoids were varied in size (small, large) and orientation (0, 45, 90 and 135 degrees). The 1 DoF reference ellipsoids had one long axis of which the size varied to be either large (0.46) or small (0.25) forming the shape of a "cigar". The 2 DoF ellipsoids had the same long axis in addition to a second axis that was half the size of the long axis. These two axes formed an "oval" in the plane of their corresponding condition. Both 1 and 2 DoF ellipsoids were rotated in their plane with either 0, 45, 90 or 135 degrees. Within each condition, every combination of size and orientation was repeated four times. The 2 DoF conditions had two additional ellipsoids, a small and large "circle" which were both repeated four times. They were not rotated within their plane, since all orientations resulted in the same compliance ellipsoid.

C. Performance measures

To measure the performance of the participants in the individual trials, we defined the completion time and three accuracy related metrics. The *Trial time* metric was defined as the time it takes for the participant to recreate the reference ellipsoid in seconds. The time started as the new reference ellipsoid spawned and was stopped by the operator when a satisfactory performance was reached. This was done by pressing a button, which also automatically spawned the next reference ellipsoid. High trial times corresponded to lower performance, and vice versa.

The accuracy of demonstrated ellipsoids was evaluated by decomposing the stiffness matrix in orientation (eigenvectors) and size (eigenvalues) components according to (4). Thus, the error between the reference and the demonstrated ellipsoid was evaluated by comparing the eigenvalues and eigenvectors. The first accuracy related metric, *Absolute average size error,* s, was defined to be the average of the absolute error between the reference and the demonstrated ellipsoid axes as

$$s = \frac{1}{n} \sum_{i=1,2,3}^{n} |\sigma_{ref,i} - \sigma_{com,i}| \tag{10}$$

The second accuracy related metric, *Relative average size accuracy,* s_{acc}, was defined to be the average error between the reference and the demonstrated ellipsoid axes, relative to the reference ellipsoid. Additionally, the score was converted to a percentage such that it could be presented to the operator as a convenient feedback score during the trials. The score ranged between $0-100\%$, where 100% represented a perfect match in size, and was defined as

$$s_{acc} = 100 - \frac{1}{n} \sum_{i=1,2,3}^{n} \left\{ \frac{|\sigma_{ref,i} - \sigma_{com,i}|}{\sigma_{ref,i}} \times 100 \right\} \tag{11}$$

The third accuracy related metric, *Orientation error,* α, was defined as the smallest absolute angle between the reference orientation and the demonstrated orientation for an arbitrary axis in the axis angle framework. The absolute angle was derived from a distance metric for 3D rotations by using the inner product of a unit quaternion ϕ [24] as

$$\phi = \arccos\left(|\boldsymbol{q}_{ref} \cdot \boldsymbol{q}_{com}|\right) \tag{12}$$

The distance metric ϕ was scaled by a factor to represent the angle in radians. Subsequently, because of the symmetry of the ellipsoid, the range was halved to $[0 - \frac{\pi}{2}\ rad]$ as

$$\alpha = \begin{cases} \pi - 2\phi & 2\phi > \frac{\pi}{2} \\ 2\phi, & \text{otherwise} \end{cases} \tag{13}$$

The angle α was also represented as a feedback accuracy score α_{acc} to the operator in (14). Similar to the size accuracy, 100% represented a perfect match in orientation. The feedback score was identical to α, only scaled to have a different range $[0 - 100\%]$ as

$$\alpha_{acc} = 100 - (\alpha \frac{2}{\pi} \times 100) \tag{14}$$

IV. Results

We performed a statistical analysis to test the null hypothesis H_0 (i.e., equal medians) of the different conditions using the Wilcoxon signed-rank test. The results of comparing the performance of commanded DoF (1 vs 2), plane (horizontal vs vertical), and size (large vs small) are presented in Table I. Additionally, Fig. 4 visualises the most important quantitative and subjective results.

Comparing 1 DoF commands with 2 DoF commands, Table I, Fig. 4a and Fig. 4b show that all metrics are significant with $p < 0.001$. As hypothesised, all median values show higher performance scores in 1 DoF compared to 2 DoF, confirming the first hypothesis.

Secondly, it was hypothesised that performance in the horizontal plane is lower compared to the performance in the vertical plane for all the performance metrics. As indicated in the legend of Fig. 4a and Fig. 4b, statistical difference is observed only for the orientation error $p < 0.001$. Furthermore, Table I reveals that the absolute and relative average size error $p = 0.73$, $p = 0.14$, are not statistically significant. Therefore, the performance in the horizontal plane is lower compared to the performance in the vertical plane, because it took the operator less time to demonstrate an ellipsoid (trial time $p < 0.001$). Furthermore, the demonstrated ellipsoids are less similar to their reference ellipsoid, where the error in similarity is based on the error in orientation $p < 0.001$ and not in the size of the stiffness commands.

Finally, it was hypothesised that the performance for large shapes is lower than for small shapes (for the trial time only). Table I confirms this with $p < 0.001$, however, the orientation error $p = 0.004$ and absolute average size error $p < 0.001$ also show a statistically significant difference. The median values of large shapes reveal a (small) increase in performance score in orientation error, but lower performance score in the absolute average size error.

All eight participants reported a positive experience in terms of the usefulness of the stiffness commanding method (see Fig. 4c). However, not all participants were satisfied with the stiffness commanding interface. Out of the eight participants, six participants reported a positive score, one neutral and one participant was not satisfied. Comments during the experiment and feedback from the questions as described in (III-B) indicate that force feedback was either helpful or tiring. All participants perceived the 2 DoF commands as the more difficult mode. Six participants reported that the horizontal plane was the more difficult view. Additionally, ellipsoids that are oriented diagonally between two axes with a 45 or 135 degrees rotation were considered more difficult. Finally, comments were made on the visualisations, where the orientation of small ellipsoids was difficult to see.

V. Discussion

The trial time is an indicator of overall performance for the plane and DoF conditions since it shows how quickly the participant reached satisfactory performance. It should be noted that if a subsequent trial features a differently oriented compliance ellipsoid, it took 2 seconds to rotate the

TABLE I

STATISTICAL ANALYSIS: DESCRIPTIVE STATISTICS (LEFT) AND INFERENTIAL STATISTICS (RIGHT)

		Descriptive Statistics						**Inferential Statistics**		
Metrics\Conditions		1 DoF (493)	2 DoF (493)	Horizontal (555)	Vertical (555)	Large (556)	Small (556)	1 DoF = 2 DoF	Horizontal = Vertical	Large = Small
trial time [s]	Q_2	5.68	6.88	7.06	6.14	8.22	5.60	w = 43620	w = 62291	w = 32307.5
	Q_1	3.34	4.02	4.11	3.47	4.28	3.29	**p < 0.001***	**p < 0.001***	**p < 0.001***
	Q_3	9.72	11.74	11.51	10.75	13.90	8.75			
absolute average size error [-] [0.14 - 0.33] [2]	Q_2	$0.92 \cdot 10^{-2}$	$1.49 \cdot 10^{-2}$	$1.25 \cdot 10^{-2}$	$1.27 \cdot 10^{-2}$	$1.63 \cdot 10^{-2}$	$0.98 \cdot 10^{-2}$	w = 34089	w = 75851	w = 71071.5
	Q_1	$0.45 \cdot 10^{-2}$	$0.91 \cdot 10^{-2}$	$0.74 \cdot 10^{-2}$	$0.68 \cdot 10^{-2}$	$0.94 \cdot 10^{-2}$	$0.53 \cdot 10^{-2}$	**p < 0.001***	p = 0.73	**p < 0.001***
	Q_3	$1.65 \cdot 10^{-2}$	$2.26 \cdot 10^{-2}$	$2.16 \cdot 10^{-2}$	$2.00 \cdot 10^{-2}$	$2.55 \cdot 10^{-2}$	$1.59 \cdot 10^{-2}$			
relative average size accuracy [%] [1] [0-100] [3]	Q_2	97.21	93.70	95.22	95.57	95.56	95.22	w = 18487	w = 70566	w = 32504
	Q_1	98.65	95.91	97.48	97.67	97.50	97.72	**p < 0.001***	p = 0.14	p = 0.11
	Q_3	94.99	90.06	92.29	92.86	92.75	92.15			
orientation error [deg] [0-90] [3]	Q_2	6.65	17.41	14.79	10.87	11.45	12.92	w = 15658	w = 54113	w = 66391
	Q_1	2.98	10.83	6.56	5.20	5.71	5.84	**p < 0.001***	**p < 0.001***	**p = 0.004***
	Q_3	14.13	26.09	23.87	18.26	20.34	21.96			

Q_1 is the first quartile, Q_2 is the median, and Q_3 is the third quartile of respective data sets.
[1] Different than the other metrics, high scores correspond with high performance.
[2] Presents the minimum and maximum average size of the reference ellipsoids.
[3] Presents the range of the minimum and maximum scores.
* Significant difference ($p \leq 0.05$), which rejects the null hypothesis H_0.

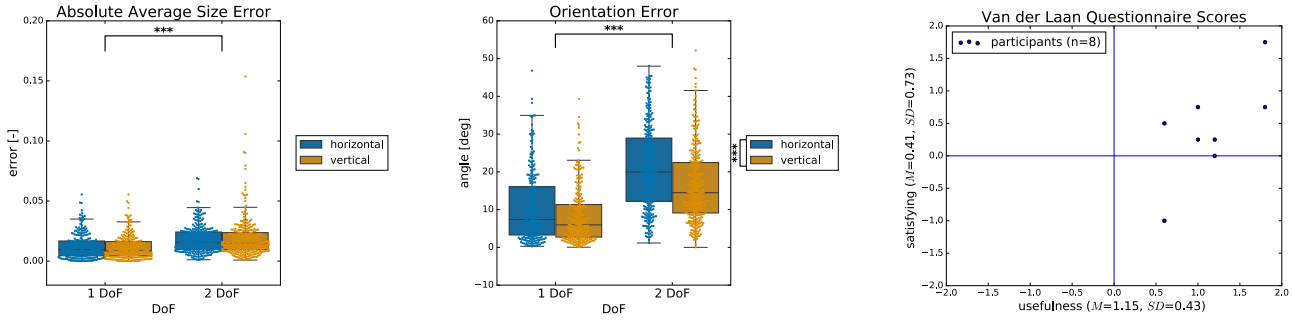

(a) (b) (c)

Fig. 4. Quantitative (a),(b) and subjective (c) results. The main metrics (a) average shape error and (b) absolute angle are compared for the commanded DoF and plane, where significance is denoted by: $* \ p \leq 0.05$, $** \ p \leq 0.01$, $*** \ p \leq 0.001$. (c) Presents the van der Laan acceptance scores [20] that evaluate the stiffness commanding method. The horizontal axis represents the usefulness scale and the vertical axis represents the satisfying scale where the self-reported scores range from -2 (negative) to 2 (positive).

compliance ellipsoid in the correct direction. Two seconds was the time needed for the temporal sliding window to have an all-new perturbation signal. The remaining time, was the time needed for the operator to reach satisfactory stiffness commands/performance.

As hypothesised, the results show that all performance metrics have significantly higher scores in 1 DoF commands compared to 2 DoF. 1 DoF command mode might be preferred when demonstrating or adjusting a specific axis magnitude of ellipsoids, since it is quick and accurate. On the other hand, using 1 DoF command mode to demonstrate multiple axes of ellipsoids, the operator has to independently and sequentially control the magnitude of individual axes, which can be less convenient. Therefore, the task and conditions at hand should dictate the choice of the mode.

Furthermore, all participants agreed that 2 DoF commands are perceived as more difficult, where additional participant feedback suggests that controlling the pitch in 2 DoF was especially difficult. In theory, the interface also allows simultaneous commanding in 3 DoF. Following the trend, increasing the DoF would even further decrease the performance and is expected to be too difficult. Therefore, we recommend multiple demonstrations in order to modulate the stiffness in 3 DoF independently.

The second hypothesis expected a decrease in performance for horizontal commands compared to vertical commands. This hypothesis is partly satisfied since the overall performance did indeed decrease. The metrics trial time and orientation error showed a significant decrease in performance, while the relative and absolute size error did not. A potential reason could be that horizontal commands required the operator to mainly focus on the less natural top-down view of the remote/simulated scene.

However, this is likely not the only effect that contributed to a difference in orientation error. Due to manipulability properties, the kinematic structure of the human arm allows for easier movements in certain directions, while being more resistant to perturbation forces in other directions [23]. Moreover, the study in [25] revealed a significant and consistent anisotropy in force magnitude perception in the three dimensional axes. Therefore, different perceptions of force (or even movement) could contribute to the difference in performance in the horizontal and vertical planes. This is even more likely, since the feedback from the participants revealed that they had more difficulties in orienting their stiffness commands along the diagonals (45 and 135 degrees

of rotation) within the horizontal or vertical plane condition.

It can be concluded that the commanded direction and/or reference view of the operator influences the performance of the stiffness commands through the eigenvectors only. Therefore, the viewpoint of the operator, direction of the stiffness commands, and alignment with the robot reference frame should be carefully considered when maximising performance for a task demonstration. Future work could try to distinguish what effects contribute the most in order to further improve the interface.

Finally, it was hypothesised that trial times for large ellipsoids are higher than small ellipsoids, which is confirmed in the results. Commands that require larger movements take naturally more time compared to small movements. However, another effect is expected to contribute to the increased trial times. User feedback reveals that the difference between the demonstrated ellipsoid and reference ellipsoid was difficult to see for small sizes. Therefore, participants could spend more time on correcting their orientation and size error for large ellipsoids, since they were more aware of these errors. This is in accordance with the small significant decrease in orientation error for large sizes, which suggests that participants were able to improve performance on orientation, when allowed more time and improved visuals.

Furthermore, the results show that the error in absolute size is significantly greater for large shapes, while the relative size error is not. Large sizes result in a larger absolute over and undershoot, but are in proportion to the size of the reference ellipsoid.

The van der Laan acceptance score indicated that the method was perceived as useful and intuitive. However, not everybody was satisfied. Participant feedback clarifies that participants either liked or disliked the force feedback. Additionally, some participants reported that the force feedback becomes tiring after a while. Depending on the participant, the experiment time ranged between 45 and 75 minutes. Since the method is intended for learning impedance behaviour, it is unlikely that stiffness will be commanded for such long periods. To increase user satisfaction, the most simple solution would be to lower the force feedback to prevent the operators from getting tired. Instead, the forces can be visualised on the screen.

REFERENCES

[1] N. Hogan, "Impedance control - An approach to manipulation. I - Theory. II - Implementation. III - Applications," *ASME Transactions Journal of Dynamic Systems and Measurement Control B*, vol. 107, pp. 1–24, Mar. 1985.

[2] F. J. Abu-Dakka, L. Rozo, and D. G. Caldwell, "Force-based variable impedance learning for robotic manipulation," *Robotics and Autonomous Systems*, vol. 109, pp. 156–167, 2018.

[3] S. Calinon, I. Sardellitti, and D. G. Caldwell, "Learning-based control strategy for safe human-robot interaction exploiting task and robot redundancies," in *2010 IEEE/RSJ International Conference on Intelligent Robots and Systems*, 2010, pp. 249–254.

[4] P. Kormushev, S. Calinon, and D. G. Caldwell, "Imitation learning of positional and force skills demonstrated via kinesthetic teaching and haptic input," *Advanced Robotics*, vol. 25, no. 5, pp. 581–603, 2011.

[5] L. Peternel, T. Petrič, and J. Babič, "Robotic assembly solution by human-in-the-loop teaching method based on real-time stiffness modulation," *Autonomous Robots*, vol. 42, no. 1, pp. 1–17, 2018.

[6] A. Pervez, A. Ali, J.-H. Ryu, and D. Lee, "Novel learning from demonstration approach for repetitive teleoperation tasks," in *2017 IEEE World Haptics Conference*, 2017, pp. 60–65.

[7] M. Suomalainen, J. Koivumäki, S. Lampinen, V. Kyrki, and J. Mattila, "Learning from demonstration for hydraulic manipulators," in *2018 IEEE/RSJ International Conference on Intelligent Robots and Systems*, 2018, pp. 3579–3586.

[8] A. Ajoudani, N. Tsagarakis, and A. Bicchi, "Tele-impedance: Teleoperation with impedance regulation using a body–machine interface," *The International Journal of Robotics Research*, vol. 31, no. 13, pp. 1642–1656, 2012.

[9] L. Peternel, T. Petrič, E. Oztop, and J. Babič, "Teaching robots to cooperate with humans in dynamic manipulation tasks based on multi-modal human-in-the-loop approach," *Autonomous robots*, vol. 36, no. 1-2, pp. 123–136, 2014.

[10] C. Yang, C. Zeng, C. Fang, W. He, and Z. Li, "A dmps-based framework for robot learning and generalization of humanlike variable impedance skills," *IEEE/ASME Transactions on Mechatronics*, vol. 23, no. 3, pp. 1193–1203, 2018.

[11] A. Ajoudani, C. Fang, N. Tsagarakis, and A. Bicchi, "Reduced-complexity representation of the human arm active endpoint stiffness for supervisory control of remote manipulation," *The International Journal of Robotics Research*, vol. 37, no. 1, pp. 155–167, 2018.

[12] C. Yang, C. Zeng, P. Liang, Z. Li, R. Li, and C.-Y. Su, "Interface design of a physical human–robot interaction system for human impedance adaptive skill transfer," *IEEE Transactions on Automation Science and Engineering*, vol. 15, no. 1, pp. 329–340, 2017.

[13] M. Laghi, A. Ajoudani, M. Catalano, and A. Bicchi, "Tele-impedance with force feedback under communication time delay," in *2017 IEEE/RSJ International Conference on Intelligent Robots and Systems*, 2017, pp. 2564–2571.

[14] L. M. Doornebosch, D. A. Abbink, and L. Peternel, "Analysis of coupling effect in human-commanded stiffness during bilateral tele-impedance," *IEEE Transactions on Robotics*, vol. 37, no. 4, pp. 1282–1297, 2021.

[15] D. S. Walker, R. P. Wilson, and G. Niemeyer, "User-controlled variable impedance teleoperation," in *2010 IEEE International Conference on Robotics and Automation*, 2010, pp. 5352–5357.

[16] K. Kronander and A. Billard, "Online learning of varying stiffness through physical human-robot interaction," in *2012 IEEE International Conference on Robotics and Automation*, 2012, pp. 1842–1849.

[17] ——, "Learning compliant manipulation through kinesthetic and tactile human-robot interaction," *IEEE transactions on haptics*, vol. 7, no. 3, pp. 367–380, 2014.

[18] V. Ho, C. Borst, M. M. van Paassen, and M. Mulder, "Increasing acceptance of haptic feedback in uav teleoperation by visualizing force fields," in *2018 IEEE International Conference on Systems, Man, and Cybernetics (SMC)*, 2018, pp. 3027–3032.

[19] W. Vreugdenhil, S. Barendswaard, D. A. Abbink, C. Borst, and S. M. Petermeijer, "Complementing haptic shared control with visual feedback for obstacle avoidance," *IFAC-PapersOnLine*, vol. 52, no. 19, pp. 371–376, 2019.

[20] J. D. Van Der Laan, A. Heino, and D. De Waard, "A simple procedure for the assessment of acceptance of advanced transport telematics," *Transportation Research Part C: Emerging Technologies*, vol. 5, no. 1, pp. 1–10, 1997.

[21] R. E. Wood, "Task complexity: Definition of the construct," *Organizational behavior and human decision processes*, vol. 37, no. 1, pp. 60–82, 1986.

[22] B. P. DeJong, J. E. Colgate, and M. A. Peshkin, "Improving teleoperation: reducing mental rotations and translations," in *2004 IEEE International Conference on Robotics and Automation*, vol. 4, 2004, pp. 3708–3714.

[23] W. Kim, L. Peternel, M. Lorenzini, J. Babič, and A. Ajoudani, "A human-robot collaboration framework for improving ergonomics during dexterous operation of power tools," *Robotics and Computer-Integrated Manufacturing*, vol. 68, p. 102084, 2021.

[24] D. Q. Huynh, "Metrics for 3d rotations: Comparison and analysis," *Journal of Mathematical Imaging and Vision*, vol. 35, no. 2, pp. 155–164, 2009.

[25] F. E. Van Beek, W. M. B. Tiest, W. Mugge, and A. M. Kappers, "Haptic perception of force magnitude and its relation to postural arm dynamics in 3d," *Scientific reports*, vol. 5, no. 1, pp. 1–11, 2015.